Journal of Microbiology, Immunology and Infection 56 (2023) 257–266

Available online at www.sciencedirect.com

ScienceDirect

journal homepage: www.e-jmii.com

Original Article

The trajectory patterns of single HIV-1 virus-like particle in live CD4 cells: A real time three-dimensional multi-resolution microscopy study using encapsulated nonblinking giant quantum dot

Wei-You Li [a], Shuhui Yin [c], Szu-Wei Huang [d], Ming-Hui Yang [e], Patricia MT. Chen [f], Shang-Rung Wu [g], Kevin Welsher [h], Haw Yang [c,**], Yi-Ming Arthur Chen [a,b,i,*]

[a] *Laboratory of Important Infectious Diseases and Cancer, Department of Medicine, School of Medicine, Fu Jen Catholic University, New Taipei City 242, Taiwan*
[b] *School of Medicine, Fu Jen Catholic University, New Taipei City 242, Taiwan*
[c] *Department of Chemistry, Princeton University, Princeton, NJ 08544, USA*
[d] *Division of Infectious Diseases, Anschutz Medical Campus, University of Colorado School of Medicine, Aurora, CO, 80045, USA*
[e] *Department of Medical Education and Research, Kaohsiung Veterans General Hospital, Kaohsiung 813, Taiwan*
[f] *College of Medicine, California Northstate University, Elk Grove, CA 95757, USA*
[g] *Institute of Oral Medicine, National Cheng Kung University, Tainan 701, Taiwan*
[h] *French Family Science Center, Department of Chemistry, 124 Science Drive, Duke University, Durham, NC 27708, USA*
[i] *National Institute of Infectious Diseases and Vaccinology, National Health Research Institutes, Miaoli County 350, Taiwan*

Received 3 May 2022; received in revised form 24 July 2022; accepted 14 August 2022
Available online 28 August 2022

KEYWORDS
HIV-1;
Quantum dots;
Single virus tracking;

Abstract *Background:* The exploration of virology knowledge was limited by the optical technology for the observation of virus. Previously, a three-dimensional multi-resolution real-time microscope system (3D-MRM) was developed to observe the uptake of HIV-1-tat peptide-modified nanoparticles in cell membrane. In this study, we labeled HIV-1 virus-like

* Corresponding author. Department of Medicine, School of Medicine and Graduate Institute of Biomedical and Pharmaceutical Science, Fu Jen Catholic University, New Taipei City 242, Taiwan. Fax: +886 2 29053415.
** Corresponding author.
E-mail addresses: hawyang@princeton.edu (H. Yang), 150110@mail.fju.edu.tw (Y.-M. Arthur Chen).

https://doi.org/10.1016/j.jmii.2022.08.011

Three-dimensional multi-resolution microscope;
Virus-like particle

particles (VLPs) with passivated giant quantum dots (gQDs) and recorded their interactive trajectories with human Jurkat CD4 cells through 3D-MRM.
Methods: The labeled of gQDs of the HIV-1 VLPs in sucrose-gradient purified viral lysates was first confirmed by Cryo-electronic microscopy and Western blot assay. After the infection with CD4 cells, the gQD-labeled VLPs were visualized and their extracellular and intracellular trajectories were recorded by 3D-MRM.
Results: A total of 208 prime trajectories was identified and classified into three distinct patterns: cell-free random diffusion pattern, directional movement pattern and cell-associated movement pattern, with distributions and mean durations were 72.6%/87.6 s, 9.1%/402.7 s and 18.3%/68.7 s, respectively. Further analysis of the spatial—temporal relationship between VLP trajectories and CD4 cells revealed the three stages of interactions: (1) cell-associated (extracellular) diffusion stage, (2) cell membrane surfing stage and (3) intracellular directional movement stage.
Conclusion: A complete trajectory of HIV-1 VLP interacting with CD4 cells was presented in animation. This encapsulating method could increase the accuracy for the observation of HIV-1-CD4 cell interaction in real time and three dimensions.

Introduction

A mechanistic understanding of the interaction between viruses and their host, especially at the cellular level is essential to the prevention and treatment of viral diseases. Virus is generally smaller than the diffraction limit and out of the resolution range of optical microscopes, which leads to limitations in its observation and investigation.[1] In 1980s, researchers used fluorescent probes to label single virus and fluorescent probes have since become the main molecules to track single VLP movement in live-cell.[2—5] Though providing only approximate and indirect evidence, this method allowed researchers to gather important information on the spatial relationship between viral particles and host cells.[6] For example, Miyauchi et al. used green fluorescent protein (GFP) tagged VLP combined with lipophilic dye to demonstrate that HIV-1 VLP could be internalized within human CD4 monocytes via a ligand-receptor triggered endocytosis pathway.[7,8] However, intrinsic shortcomings, such as insufficient dynamic range and photon emitting quantity caused by the transient lifetime during photobleaching, hinder the application of fluorescent probes in virology research.[9] Photobleaching of a fluorophore is due to photon-induced irreversible molecular structural damage during the photon-absorption/emission cycle.[10] While under a saturated excitation state, fluorophore-based probes typically only emit 10^4-10^5 photons before reaching a photobleached state.[11] These limitations obstruct the achievement of the real-time single virus tracking in live-cells. Quantum dots (QDs) are nano-sized semiconductor particles that possess optoelectronic property and high bio-compatibility. The number of photons emitted by QDs before photobleaching via photon-oxidation is approximately 10^8 photons, which is robust enough to take on a significantly higher number of absorption/emission cycles and maintain sufficient lifetime in live-cell observation.[12,13] The application of QDs in the field of virology research has seen an exponential increase in the past decade. Researchers have used QDs to demonstrate the adhesion of HIV-1 VLPs on the cell membrane surface of host cells in real time.[1,14] Recently, QDs were also successfully encapsulated into enveloped virus in living cells and used to track viral infections.[15] These results have shown that QDs conjugated with modified genomic RNA are capable of being encapsulated into the capsid of vesicular stomatitis virus, a glycoprotein pseudotyped lentivirus.

The resolution limit of microscopy technique presents another challenge to study single virus tracking. For instance, the imaging resolutions of structured illumination microscopy and stimulated emission depletion microscopy are limited to 225 nM and 80 nM, respectively.[5] This greatly limits the acquisition of detail information between virus—cell interaction and the reconstruction of the infection scenario. In order to overcome these limitations, an advanced strategy utilizing encapsulated nonblinking giant quantum-dots (gQDs) has been shown to provide a higher photostability and luminosity signal in the cavity of HIV-1 VLP.[16]

Previously, we demonstrated that the trajectory of a HIV-Tat-modified nanoparticle, presented as a "kiss and run" pattern, could be acquired via a recently developed 3D-MRM system.[17] In the current study, we designed and cloned an octa-histidine tagged pCMVΔR8.91 (pCMVΔR8.91-8his) to generate an HIV-1 VLPs that can be labelled by gQDs.[18] We then used the 3D-MRM to visualize the multi-scale process of VLPs attachment and internalization. This 3D-MRM device provides 3D spatial positioning information for gQD-encapsulated HIV-1 VLPs (gQD-HIV-1 VLPs) with a high resolution of approximately 10 nm. Our methodology not only collects background landscape images of the infection locus between host cells via a two-photon laser scanning confocal microscope, but also reconstitute the

infection-associated VLP's trajectory and whole background landscape of host cells.

Methods

Cell-lines and plasmids

HeLa cells and Jurkat T cells (harboring the CD4 T-cell receptor) were obtained from American Type Culture Collection. The maintained of HeLa cells and Jurkat cells has been described previously.[19,20] We constructed the pCMVΔR8.91-8his lentiviral vector from pCMVΔR8.91 after amplifying a repeated histidine tag and an additional segment containing protease cutting site by polymerase chain reaction (PCR) and inserting it between matrix protein and capsid protein in the *gag* region of the vector. The additional protease segment flanked with the 8-his tag sequence (SQNYPIVQ-8-histidine-QNYPIVQ, 1815—1881).

gQDs preparation and electroporation

CdSe/CdS core/shell gQDs were synthesized as described before.[21] In brief, 322 mg of diphenylphospine selenium (DPPSe) and 128 mg of CdO were prepared individually in the beginning as the precursor of selenium and cadmium. Then the nucleation procedure was conducted after the combination of two precursors in certain condition, followed by centrifugation (4000×*g*, 10 min). The harvested gQDs were passivated with m-dPEG12-Lipoamide (Quanta BioDesign) by following a previously reported procedure.[22] The passivated gQDs were then dissolved in 400 μL BTXpress high performance electroporation solution (BTX, USA) and mixed with 2×10^6 Hela cells in a cuvette and kept on ice for 7 min. The cuvette was inserted into a BTX ECM 830 electroporation system (BTX, USA), gQDs electroporation was conducted at 300 V, 2 ms and square wave mode. After 2 min on ice incubation, gQDs electroporated cells were re-dissolved by 10 mL 10% FBS containing DMEM (Bio-Science, Ireland), seeded into a 100 mm cell culture dish (Nunc, USA), and incubated overnight at 37 °C.

gQD-HIV-1 VLPs preparation and concentration

The gQD-HIV-1 VLPs were generated from the gQDs-electroporated Hela cells which were co-transfected by pCMVΔR8.91-8His, the packaging plasmid, and pHXB2-env envelop expression plasmids via Lipofectamine 3000 (Thermo Fisher Scientific, USA). Transfection was performed by following the instructions provided by the manufacturer. After 48hr at 37 °C incubation, the culture supernatant was collected in an Open-Top ultracentrifuge tube (Beckman Coulter, USA). 20% Sucrose solution (Sigma Aldrich, USA) was added for VLPs condensation. The ultracentrifuge procedure was performed via SW 28 Ti rotor (Beckman Coulter, USA) set at 35,000 rpm, 1h and 4 °C, slow brake. The pellets were retrieved by 10 μL phosphate buffered saline (PBS).

Western blotting

The details of the Western blot have been described previously.[23] HIV-1 Gag p55 precursor protein and capsid p24 protein were detected by anti-p24gag mouse monoclonal antibody (clone 183-H12-5C).[24] Histidine was detected by anti-6X His tag mouse monoclonal antibody (Abcam, USA). The detection of primary antibody was performed using horseradish peroxidase (HRP)-conjugated secondary antibody (goat anti-mouse IgG, Amersham Biosciences, UK). The intensity quantification of reactive bands in Western blot was analyzed via Image J software (ver. 1.8.0_112, National Institutes of Health, USA).

Transmission electron microscopy (TEM) and cryogenic electron microscopy (Cryo-EM)

5 μL of concentrated VLPs solution were dropped on the TEM grid (Ted Pella Inc., USA) for 1min RT incubation. The remaining VLPs sample was wiped out via a filter paper and 10 μL 2% paraformaldehyde (Sigma Aldrich, USA) were dropped on the grid for fixation. 30 s later, the grid was washed by 15 μL ddH_2O three times. The grid was negatively stained by 2% OSO4 (Sigma Aldrich, USA) and 2% uranyl acetate (Sigma Aldrich, USA). After staining the grid, wash and air-dry followed. The TEM images of VLPs were captured by Zeiss EM 912 TEM (Zeiss, Germany). The sample preparation for Cryo-EM has been described previously and a JEM-2100 F TEM (JEOL, Japan) was used.[25]

The single gQD-HIV-1 VLP real-time tracking and image reconstruction

A 3D-MRM system was used for gQD-HIV-1 VLPs real-time tracking. It was accomplished by the combination of a temperature control system, 642-nm CW diode laser, sapphire laser, 3D piezoelectric stage, two-photon laser scanning microscope (LSM 410, LSM Tech), an Electron Multiplying Charge Coupled Device (Photometrics Cascade 512 B), Avalanche photodiodes of three different directions (X, Y and Z), three photomultiplier tubes, and an associated set of light path modules. All the subsystems worked to create a micro adjustment to move the 3D piezoelectric stage immediately so as to track the motion of single nanoparticles within a lower-resolution 3D context in real time. In order to mimic the natural scenario of HIV-1 infection, Jurkat cells from a human acute T cell leukemia cell-line were used as host cells during the VLP observation and tracking period. 1.1×10^6 Jurkat cells were stained with 2.25 μM SYTO 41 (Invitrogen, USA) at 37 °C and incubated for 20 min. Cell pellets were dissolved in 1 mL RPMI medium, seeded into a 500 kDa poly-D-lysine (50 μg/mL, BD Biosciences, USA) coated Delta-T glass bottom dish (Biotechs, USA), and centrifuged at 2500 rpm for 5 min (for cell adhesion). After that, the medium was replaced with 350 μL virus-contained PBS (10% FBS, 10 μL gQD-VLPs solution and 8 μg/mL polybrene, sigma), and incubated at 4 °C for 10 min before tracking. Following our previous design,[17] the multiple imagine stacks which had been taken

with a two-photon laser scanning microscope synchronously with the gQDs trajectory record were used. The 3D cell-surfaces and micro environment were reconstructed using the isosurface rendering function in MATLAB software. For the definition of prime trajectories of gQD-HIV-1-VLPs that had been identified through 3D-MRM, three distinct patterns were classified based on the definitions below: the maximum displacement of trajectories on any axis of less than 1.4 μm and without regular direction or pattern was defined as cell-free random diffusion pattern (CFRD); the maximum displacement of trajectories on any axis of more than 1.4 μm and present in the same direction was defined as directional movement pattern (DM); the maximum displacement of trajectories on any axis of more than 1.4 μm and present in an irregular or multi-directional pattern was defined as cell-associated movement pattern (CAM).

Results

The preparation and verification of gQD-HIV-1 VLPs

In order to track the movement of a single VLP in real-time, we established the HIV-1VLPs labeled with gQDs. Based on the chelation effect between long repeat histidine and gQDs, an eight-histidine (8-his) tag expressed pCMVΔR8.91 vector was designed and cloned. As shown by the gQD-HIV-1 VLPs generation flow chart (Fig. 1A), after co-transfected with both the pCMVΔR8.91-8his and pHXB2 *env* plasmids, HeLa cells were electroporated with gQDs. The gQDs then could be chelated by the 8-his tag of the pCMVΔR8.91-8his plasmids in the cytoplasm during the *gag-pol* polyprotein assembly process. And, subsequently, the gQDs-labeled *gag* polyprotein could be packaged into the VLPs. Along with the VLPs budding, the gQD-8-his chelation complex were released into the space between the capsid and plasma membrane after VLPs maturation. The generation of HIV-1 VLPs was confirmed by Western blot analysis for the expression of HIV-1 *gag* polyprotein (p55) and histidine (Fig. 1B). In order to achieve the specific gravity changes and gQDs encapsulation ratios within the same batch of VLPs, differential ultra-centrifugation utilizing sucrose gradient was conducted to separate VLPs by their specific gravity in different concentrations of sucrose (20%—80%). The separation of gQD-HIV-1 VLPs were further examined by Western blot analysis for the expression of HIV-1 p55 protein. As shown in Fig. 1C, in comparison to most of the gQD (−) 8-his-HIV-1 VLPs being residing within 1st to 4th fractions (20—40% sucrose solution), the gQD (+) 8-his-HIV-1VLPs displayed a distribution "shift" toward the 4th-to-6th fractions (40%—60% sucrose, density = 1.286). This shift conceivably reflects the expected increase in specific gravity of the HIV-1 VLPs after gQDs-encapsulation. Furthermore, the relative expression level of p55 of each fraction was quantified to show the distribution of HIV-1 VLPs with and without gQD encapsulation. As shown in Fig. 1D, the ratio of gQDs encapsulation within 8-his-HIV-1 VLPs during our VLPs generation procedure was about 17.14% (calculated by summing the relative ratios of the 5th to 6th fractions of HIV p55 protein).

To further verify gQD encapsulation in VLPs carrying eight-histidine (8-his) tags, fluorescence microscopy was conducted to study VLPs-containing supernatant collected from HeLa cells prepared in four different conditions: (A) gQDs delivered by electroporation without transfection (QD only), (B) pCMVΔR8.91-8-his and pHXB2 *env* transfection without gQDs delivered (8-his-HIV-1 VLPs), (C) pCMVΔR8.91 and pHXB2 *env* co-transfection with gQDs delivered (QD + WT HIV-1 VLPs), and (D) pCMVΔR8.91-8-his and pHXB2 *env* transfection with gQDs delivered (QD + 8-his-HIV-1 VLPs). As shown in Fig. 2A—D, under the same excitation intensity, significant gQDs signals were observed exclusively in the supernatant prepared from Hela cells co-transfected with both pCMVΔR8.91-8-his and pHXB2 *env* plasmids and with gQDs electroporation. In contrast, there were no to extremely dim signals observed in the three control supernatants prepared from Hela cells without a complete combination of gQDs electroporation and transfection of both pCMVΔR8.91-8-his and pHXB2 *env* plasmids plasmid transfection. Finally, transmission electron microscopy (TEM) and Cryo-electron microscopy (Cryo-EM) were performed to directly "visualize" the presence of gQDs encapsulation. As shown in Fig. 2E, gQDs were clearly demonstrated inside of the HIV-1 VLPs by both TEM and Cryo-EM images. These findings verify the successful preparation of gQD-HIV-1 VLPs by our research design and methodology.

The real-time tracking of gQD-HIV-1 VLPs via 3D-MRM

The 3D-MRM real-time tracking process started from the inoculation of gQD-HIV-1 VLPs with Jurkat cells. Due to the instability of gQD and cell homeostasis, the tracking time for each set of inoculated cell culture was less than 2 h. After 36 hous of continued data harvesting, a total of 208 prime trajectories were collected. These trajectories were classified into three distinct patterns: the CFRD pattern, the DM pattern, and the CAM pattern (Table 1 and Supplementary Fig. S1). According to the space-temporal information provided by the 3D-MRM, the prime trajectories in the DM or CAM patterns were further merged with the two-photon laser scanning microscopy images of host cells. These merged and 3D rendered image results showed 3 different stages of interactions between the trajectories of gQD-HIV-1-VLPs and the host cells, namely, the cell-associated extracellular diffusion stage, the membrane surfing stage, and the intracellular directional movement stage (Figs. 3 and 4). These stages were identified based on the location data of VLPs and host cells that could be acquired synchronously. Using an integrated graph from 3D-MRM space temporal information and 2 photo laser scanning microscopy, we were able to recognize the target VLPs locked in during the stage of cell-free viral infection.

In the cell-associated extracellular diffusion stage, the prime trajectories of VLPs presented in typical random Brownian motion (was characterized by mean-square-displacement analysis) when they were near the cell surface (Fig. 3A and B) or in suspended observation medium (Fig. 3C). In the membrane surfing stage, the prime trajectories of VLPa also showed membrane surfing-like

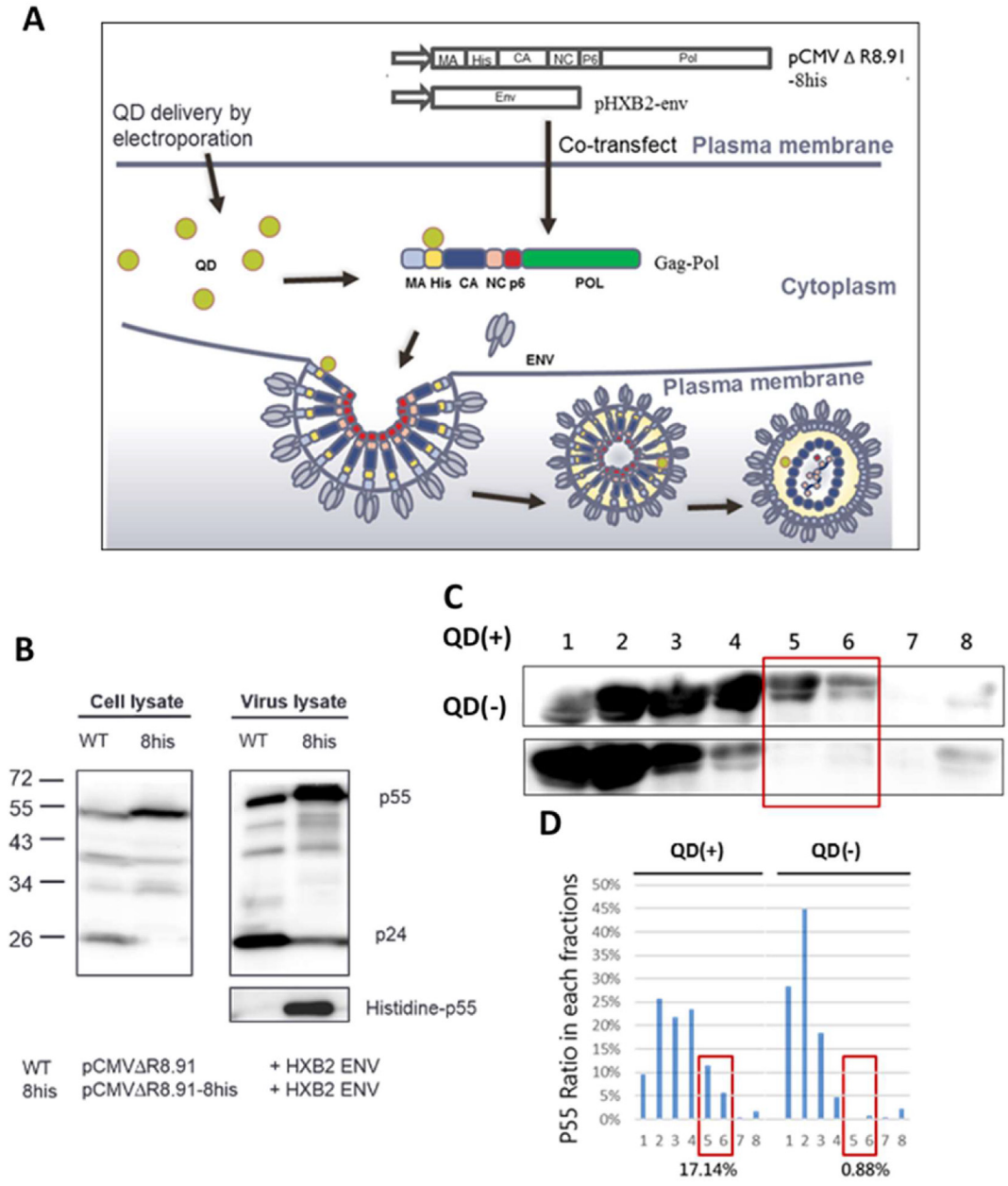

Fig. 1. The preparation of gQD-encapsulated virion. (A) Flow chart of QD-encapsulated virion generation. The pCMVΔR8.91 vector, used as a packaging plasmid in the lentivirus transfection system, contains the gag and pol region of the HIV-1 genome (600—5734). Its long terminal repeat (LTR) region was replaced by cytomegalovirus (CMV) promoter (27—614) and truncated at *env* region, psi-signal, and parts of the accessory proteins such as Vif, Vpr, and Nef. (B) Western blot analysis for the HIV-1 gag p55 and capsid p24 protein expressions of WT virion (pCMVΔR8.91 + HXB2 ENV) and 8his virion (pCMVΔR8.91-8his + HXB2 ENV) in cellular and virus lysates. (C) Western blot analysis of different density layers of sucrose gradient prepared from QD (+)/(−) 8-his virion-infected cells for the HIV-1 p55 protein expression. (D) Relative quantification bar graph from (C) demonstrates a shift of relative HIV-1 p55 protein percentage by QD-encapsulation [from 0.88% for QD (−) to 17.14% for QD (+) in the 5th to 6th fractions].

motion and presented a non-random directional movement along the edge of the cell surface accompanied with decreasing velocity (Fig. 4A and B). This kind of movement could represent the complexity of the ligand-receptor docking process. It's noteworthy that, some trajectories showed detachment of membrane after surfing-like movement (Fig. 4A), but others still remained on the membrane until the signal/movement discontinued (Fig. 4B). In addition, there were several intracellular directional movements recorded. Moreover, the gQDs signal represented in Fig. 4C and D showed a V-shape trajectory inside of a Jurkat cell, which could represent cellular process in mitosis phase.

To demonstrate the capabilities and limitations of the 3D-MRM system used in gQD-HIV-1 VLPs tracking, a complete trajectory animation of typical cell-free viral

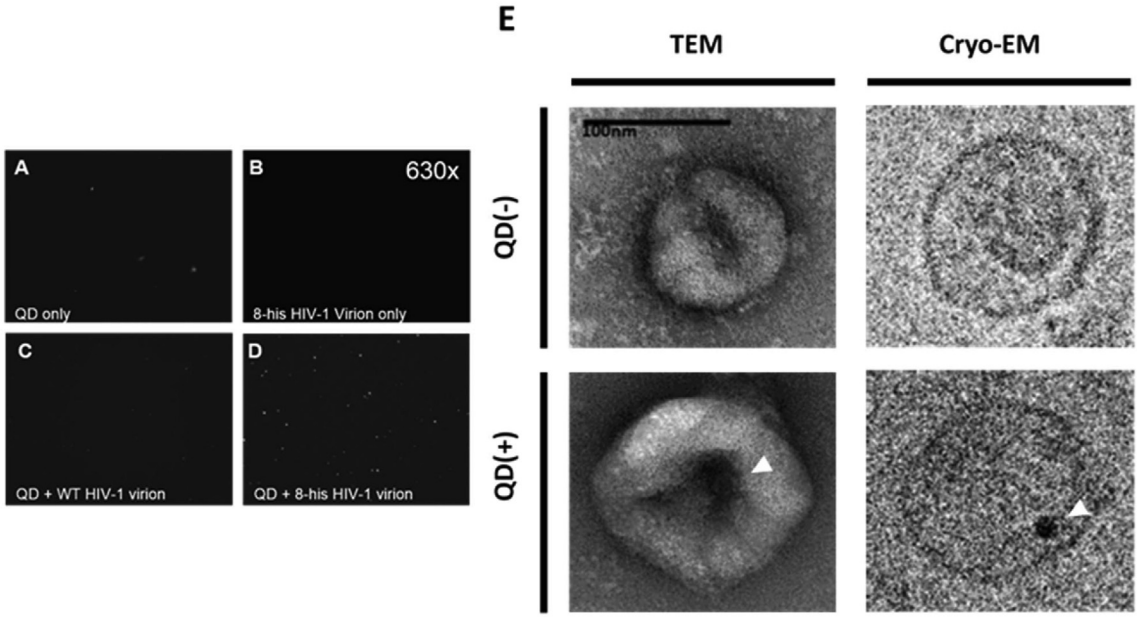

Fig. 2. The verification of gQD encapsulation in 8-his virion. (A–D) Fluorescence microscopic images of gQD (+)/(−) 8-his virion. (E) Electron microscopic images of gQD (+)/(−) 8-his virion: the lower left and lower right images are gQD-encapsulated virion visualized by transmission electron microscopy (TEM) and Cryo-electron microscopy (Cryo-EM), respectively. White arrow indicates the presence of gQD (10 nm). For comparison, both upper images are 8-his virion only without gQD.

infection was created (Fig. 4B and Supplementary Movie 1, the speed of animation had been accelerated by 5-folds approximately). There were several stages recorded during the gQDs signal lock-in within this trajectory, including the membrane-associated directional movement, membrane surface attachment and the surfing movement. In the beginning, the gQD-HIV-1 VLP was at a certain distance from the membrane of the host cell and approaching the cell membrane with a comparatively fast velocity. At the 10.52nd second, the VLP made contact with the edge of the membrane and shifted into a relative quiescent attachment phase with lower diffusion coefficients. At the 89.42nd second, the docked VLP started to move toward the membrane surface in a surfing movement pattern until the 267.82nd second.

Supplementary video related to this article can be found at https://doi.org/10.1016/j.jmii.2022.08.011

Discussion

Given the novelty and multifunctionality, the 3D-MRM and real-time tracking system can be applied to a wide variety of disciplines. To our knowledge, this is the first time the 3D-MRM was used in HIV-1 virology research. The strategy used to label viral particles in 3D-MRM system was the gQD labeling method. According to the accumulated data, the intensity and photostability of quantum dots were much higher than fluorescent proteins and other organic dyes in extracellular and intracellular conditions.[26,27] It provided longer and stronger signal after the excitation/emission reaction, making the tracking of a single particle possible.

Nevertheless, there were intrinsic limitations in gQD-labeling and gQD-passivation for our labeling strategy. Firstly, the gQD-8-his complex were cleavable by protease in the cellular system, which might have greatly hindered the observation of the full-period of infection scenario since the gQD-8-his complex could be dissociated from VLPs cavity after membrane fusion. In addition, the Western blot results in Fig. 1B clearly showed that the expression of 8-his tag diminished the production of p24 capsid protein. This may be due to the competition for protease by the additional cleavage sites along with the histidine tag expression, which could affect VLPs maturation (Fig. 1B). Secondly, random fluctuating photoluminescence phenomenon, called "blinking", may occur during the photon absorption/emission process of gQDs. This is due to photoionization and surface trap induced recombination.[13,28] The passivation process of the gQDs was limited by their own thermal sensitivity. The 37 °C incubating condition was essential to the gQD-HIV-1 VLPs preparation. This characteristic of passivation could lead to decreased stability of gQDs, resulting in "blinking" during real-time tracking,

Table 1 The frequencies and durations of three prime trajectory patterns of the gQD-HIV-1-VLPs identified by the 3D-MRM in the live Jurkat cell infection system.

Prime trajectory patterns	No. (percentage)	Mean and SD of duration (s)
Cell-free random diffusion	151 (72.6%)	87.6 ± 171.1
Directional movement	19 (9.1%)	402.7 ± 396.7
Cell-associated movement	38 (18.3%)	68.7 ± 154.5
Sum	208 (100%)	113.3 ± 218.5

which could further decrease the validity of observation and interrupt the lock-in state prematurely. Currently, there are several strategies of gQDs surface passivation in development that potentially may provide the solution to this shortcoming.[29,30]

The complete trajectory that we used to demonstrate the application of 3D-MRM in real-time VLPs tracking has presented several interesting characteristics (Fig. 4B and Supplementary Movie 1). First: Based on the distinct movement patterns and their cell—membrane association, the prime trajectories of VLPs could be separated into three stages of interactions. In our conjecture, the attachment stage began when the VLPs were physically adhered to the cell membrane and ended when the virus glycoprotein and host cell CD_4 receptor were docked together. We speculate the membrane-associated surfing movement of gQD-HIV-1 VLPs could be a random drifting process of receptor-docked VLPs in the "lipid-bilayer ocean" of the membrane surface, during which the internalization process might occur through the "meeting" of

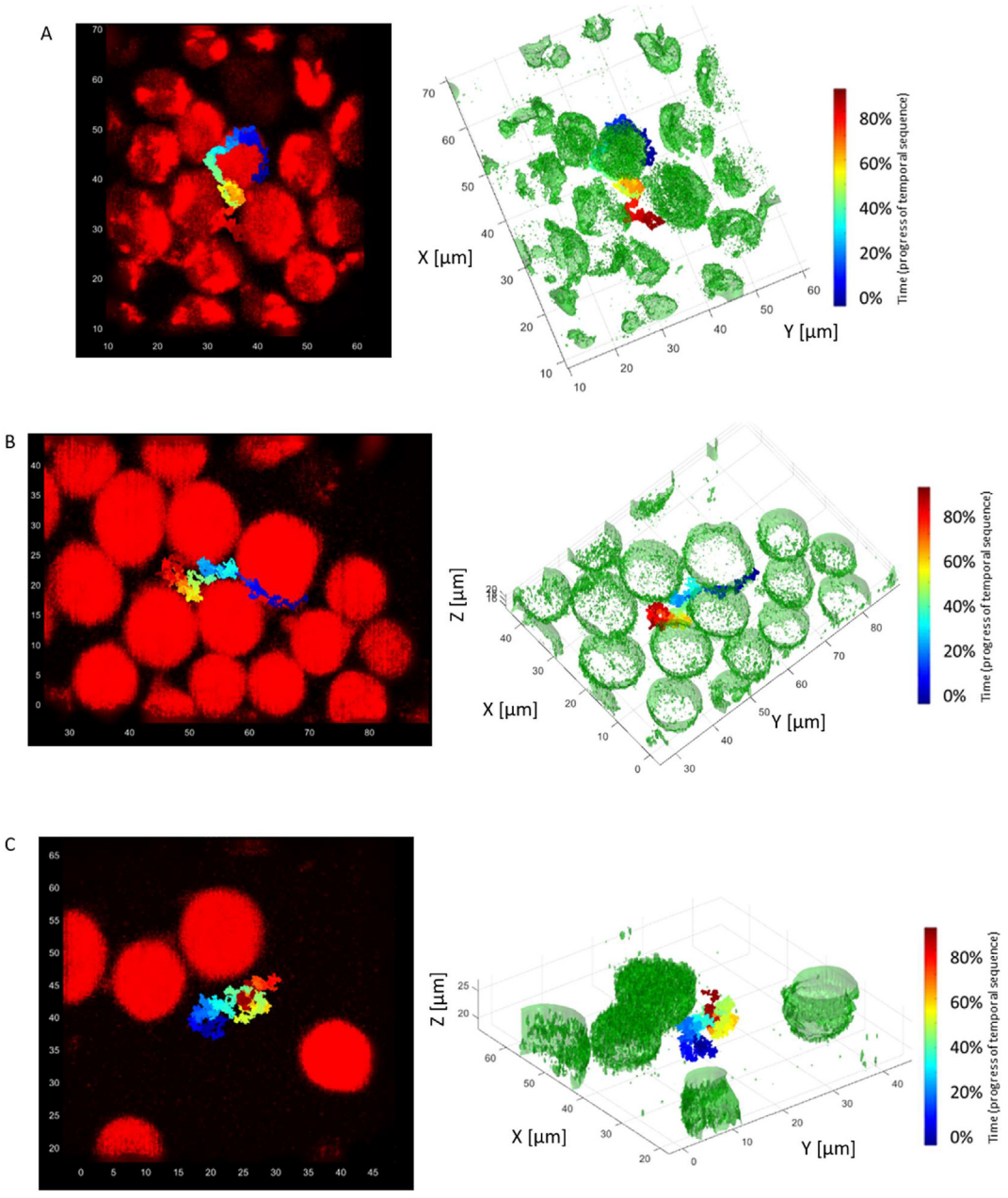

Fig. 3. Three-dimensional graph describing the extracellular diffusion stage of a gQD-HIV-1 VLP and the interaction with its target cells (Jurkat cells). (A—C) The 3D rendered image built by prime gQD-HIV-1-VLPs trajectory and cell images (left panel of each graph, acquired by two-photon laser scanning microscopy, merged with the corresponding prime trajectory images in a top view). The green color in the 3D reconstructed images indicated the rendered model of the cytoplasm of host cells. The color gradients of each trajectory starting from deep blue and ended in red represent the temporal sequence of the gQD-HIV-1-VLPs movement in the study. The red color presented in the cell images indicated the cytoplasm of host cells.

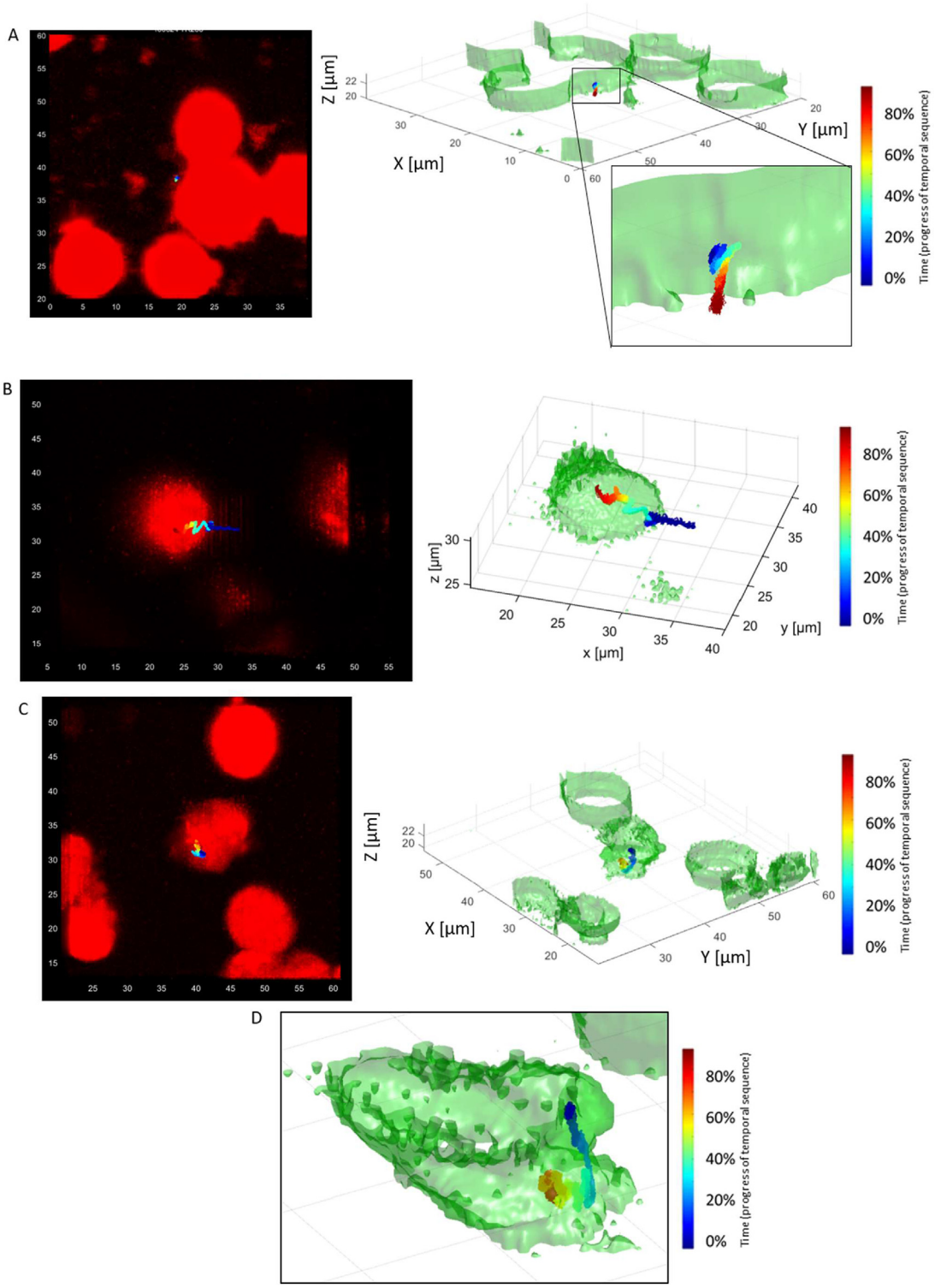

Fig. 4. Three-dimensional graph describing the cell-associated membrane surfing stage and intracellular movement stage of a gQD-HIV-1 VLP and the interaction with its target cells (Jurkat cells). (A—C) The 3D rendered image of a gQD-HIV-1 VLP trajectory in cell-associated membrane surfing stage (Fig. 4A and B) or in intracellular movement stage (Fig. 4C) built by prime trajectory and cell images (left panel of each graph, acquired by two-photon laser scanning microscopy, merged with the corresponding prime trajectory images in a top view). The lower-left panel of 4 A showed the partial enlargement image of the reconstructed image (marked by black frame). The green color in the 3D reconstructed images indicated the rendered model of the cytoplasm of host cells. The color gradients of each trajectory starting from deep blue and ended in red represent the temporal sequence of the gQD-HIV-1-VLPs movement in the study. The red color presented in the cell images indicated the cytoplasm of host cells. (D) Another view angle for the 5C trajectory and reconstructed image.

the VLP glycoprotein with its co-receptor on the cell membrane surface (CXCR4 in the case of HXB2 envelope-covered VLPs). This speculation is partly consistent with the fact that the velocity of gQD-HIV-1 VLPs decreased during the attachment phase but accelerated sequentially during the surfing movement phase. However, our data didn't present this whole process of internalization after membrane attachment and surfing motion, it is still plausible that the loss of signal is irrelevant to the entry event since possibility exists that the immediate velocity change may have interrupted the lock-in state. Nevertheless, the recorded intracellular directional trajectory strongly indicates that internalization events of gQD-HIV-1 VLPs did occur (Fig. 4C—D).

Second: The extracellular diffusion stage of this trajectory represented a sort of membrane-associated directional movement but not Brownian motion as a typical freely nano-size particle (Fig. 3). In our speculation, the membrane protrusion/filopodia of Jurkat cells may participate in this rapid and directional movement. However, the cell imaging was achieved via nucleic acid staining dye, which could not effectively recognize and visualize the actin-abundant protrusions/filopodia of the cell. Therefore, if the VLPs were surfing along with and/or interacting with the protrusion/filopodia in some way, they would seem to be moving in the extracellular space and directly toward the cell surface. Unfortunately, limitations of the hardware prohibited us to record a bright field image or to employ a second immunofluorescence dye as a visual comparison. This could potentially be improved in the future through multi-color fluorescence staining strategies or by optimizing settings.

The trajectory patterns we have demonstrated in the current study provides abundant details with unprecedented spatiotemporal information, intuitive visualization presentation, and credible 3D reconstruction of the infection scenarios. These properties are previously unable to be achieved by a conventional microscope due to its limited resolution and lack of a 3D landscape image context. With this pioneer attempt of applying 3D-MRM in virology research, given the sub-optimal labeling methodology, the current study has shown promising results. On a wider scale, the 3D-MRM coupled with encapsulated giant quantum dot technique can be applied in studies to elucidate the infection mechanism in other important human pathogens such as Dengue virus and SARS-CoV-2.

Funding sources

This work was supported by, Kaohsiung Medical University (Taiwan) and Princeton University. This research is partially supported by Kaohsiung Medical University (Taiwan) and Princeton University, sponsored by the Ministry of Science and Technology, Taiwan, R.O.C. under Grant no. MOST 110-2327-B-016-001 and by the Fu Jen Catholic University, Taiwan, R.O.C. under Grant no. 912P261-01.

Acknowledgement

The authors thank Academia Sinica (Taiwan) and Professor Chin-Tien Wang's lab, Institute of Clinical Medicine, National Yang Ming Chiao Tung University, for providing plasmids, thank Prof. Dar-Bin Shieh (Institute of Oral Medicine, National Cheng Kung University, Taiwan) for assistance with cryo-EM and Dr. Marcelo Chen (Department of Urology, MacKay Memorial Hospital, Taiwan) for writing suggestion. The authors also thank Dr. Peter Shao (Princeton Institute for the Science and Technology of Materials) for assistance with TEM, Prof. Thomas Shenk (Department of Molecular Biology, Princeton University) and Prof. Alexander Ploss (Department of Molecular Biology, Princeton University) for ultracentrifuge facilities. Szu-Wei Huang was supported by a Cancer Research Training Award from the National Cancer Institute(NCI). The content of this publication does not necessarily reflect the views or policies of the NCI, National Institutes of Health, or Department of Health and Human Services, nor does mention of trade names, commercial products, or organizations imply endorsement by the U.S. Government.

References

1. Vieweger M, Goicochea N, Koh ES, Dragnea B. Photothermal imaging and measurement of protein shell stoichiometry of single HIV-1 Gag virus-like nanoparticles. *ACS Nano* 2011;**5**(9):7324—33.
2. Helenius A, Kartenbeck J, Simons K, Fries E. On the entry of Semliki forest virus into BHK-21 cells. *J Cell Biol* 1980;**84**(2):404—20.
3. Walsh EE, Hruska J. Monoclonal antibodies to respiratory syncytial virus proteins: identification of the fusion protein. *J Virol* 1983;**47**(1):171—7.
4. Gutierrez-Granados S, Cervera L, Godia F, Carrillo J, Segura MM. Development and validation of a quantitation assay for fluorescently tagged HIV-1 virus-like particles. *J Virol Methods* 2013;**193**(1):85—95.
5. Dale BM, McNerney GP, Hubner W, Huser TR, Chen BK. Tracking and quantitation of fluorescent HIV during cell-to-cell transmission. *Methods* 2011;**53**(1):20—6.
6. Hermle J, Anders M, Heuser AM, Muller B. A simple fluorescence based assay for quantification of human immunodeficiency virus particle release. *BMC Biotechnol* 2010;**10**:32.
7. Daecke J, Fackler OT, Dittmar MT, Krausslich HG. Involvement of clathrin-mediated endocytosis in human immunodeficiency virus type 1 entry. *J Virol* 2005;**79**(3):1581—94.
8. Miyauchi K, Kim Y, Latinovic O, Morozov V, Melikyan GB. HIV enters cells via endocytosis and dynamin-dependent fusion with endosomes. *Cell* 2009;**137**(3):433—44.
9. Harms GS, Cognet L, Lommerse PH, Blab GA, Schmidt T. Autofluorescent proteins in single-molecule research: applications to live cell imaging microscopy. *Biophys J* 2001;**80**(5):2396—408.
10. HelenBridle. *Waterborne pathogens-detection methods and applications*. Academic Press; 2014. p. 416.
11. Eggeling C, Widengren J, Rigler R, Seidel CA. Photobleaching of fluorescent dyes under conditions used for single-molecule detection: evidence of two-step photolysis. *Anal Chem* 1998;**70**(13):2651—9.
12. van Sark WGJHM, Frederix PLTM, Bol AA, Gerritsen HC, Meijerink A. Blueing, bleaching, and blinking of single CdSe/ZnS quantum dots. *ChemPhysChem* 2002;**3**(10):871—9.
13. Yang C, Zhang G, Feng L, Li B, Li Z, Chen R, et al. Suppressing the photobleaching and photoluminescence intermittency of single near-infrared CdSeTe/ZnS quantum dots with p-phenylenediamine. *Opt Express* 2018;**26**(9):11889—902.

14. Jun S, Ke D, Debiec K, Zhao G, Meng X, Ambrose Z, et al. Direct visualization of HIV-1 with correlative live-cell microscopy and cryo-electron tomography. *Structure* 2011;**19**(11):1573—81.
15. Zhang Y, Ke X, Zheng Z, Zhang C, Zhang Z, Zhang F, et al. Encapsulating quantum dots into enveloped virus in living cells for tracking virus infection. *ACS Nano* 2013;**7**(5):3896—904.
16. Ghosh Y, Mangum BD, Casson JL, Williams DJ, Htoon H, Hollingsworth JA. New insights into the complexities of shell growth and the strong influence of particle volume in non-blinking "giant" core/shell nanocrystal quantum dots. *J Am Chem Soc* 2012;**134**(23):9634—43.
17. Welsher K, Yang H. Multi-resolution 3D visualization of the early stages of cellular uptake of peptide-coated nanoparticles. *Nat Nanotechnol* 2014;**9**(3):198—203.
18. Zufferey R, Nagy D, Mandel RJ, Naldini L, Trono D. Multiply attenuated lentiviral vector achieves efficient gene delivery in vivo. *Nat Biotechnol* 1997;**15**(9):871—5.
19. Lee CW, Leu SJ, Tzeng RY, Wang SF, Tsai SC, Sun KH, et al. Latent membrane protein 1 of Epstein-Barr virus regulates death-associated protein kinase 1 in lymphoblastoid cell line. *Virology* 2011;**413**(1):19—25.
20. Wang SF, Tseng SP, Huang SW, Yen CH, Hong YW, Chen M, et al. Mitochondria polarization in the contact regions of virus-infected effector cells during cell-to-cell transmission of HIV-1. *AIDS Res Hum Retrovir* 2015;**31**(2):175—6.
21. Welsher K, McManus SA, Hsia CH, Yin SH, Yang H. Discovery of protein- and DNA-imperceptible nanoparticle hard coating using gel-based reaction tuning. *J Am Chem Soc* 2015;**137**(2):580—3.
22. Emerson NT, Hsia CH, Rafalska-Metcalf IU, Yang H. Mechano-delivery of nanoparticles to the cytoplasm of living cells. *Nanoscale* 2014;**6**(9):4538—43.
23. Chiu HC, Wang FD, Chen YMA, Wang CT. Effects of human immunodeficiency virus type 1 transframe protein p6*mutations on viral protease-mediated Gag processing. *J Gen Virol* 2006;**87**:2041—6.
24. Hizi A, Tal R, Hughes SH. Mutational analysis of the DNA-polymerase and ribonuclease-H activities of human-immunodeficiency-virus type-2 reverse-transcriptase expressed in Escherichia-coli. *Virology* 1991;**180**(1):339—46.
25. Liu CC, Wu SC, Wu SR, Lin HY, Guo MS, Yung-Chih Hu A, et al. Enhancing enterovirus A71 vaccine production yield by microcarrier profusion bioreactor culture. *Vaccine* 2018;**36**(22):3134—9.
26. Ma J, Chen JY, Guo J, Wang CC, Yang WL, Xu L, et al. Photostability of thiol-capped CdTe quantum dots in living cells: the effect of photo-oxidation. *Nanotechnology* 2006;**17**(9):2083—9.
27. Vu TQ, Lam WY, Hatch EW, Lidke DS. Quantum dots for quantitative imaging: from single molecules to tissue. *Cell Tissue Res* 2015;**360**(1):71—86.
28. Yuan G, Gomez DE, Kirkwood N, Boldt K, Mulvaney P. Two mechanisms determine quantum dot blinking. *ACS Nano* 2018;**12**(4):3397—405.
29. Hohng S, Ha T. Near-complete suppression of quantum dot blinking in ambient conditions. *J Am Chem Soc* 2004;**126**(5):1324—5.
30. Roy D, Mandal S, De CK, Kumar K, Mandal PK. Nearly suppressed photoluminescence blinking of small-sized, blue-green-orange-red emitting single CdSe-based core/gradient alloy shell/shell quantum dots: correlation between truncation time and photoluminescence quantum yield. *Phys Chem Chem Phys* 2018;**20**(15):10332—44.

Appendix A. Supplementary data

Supplementary data to this article can be found online at https://doi.org/10.1016/j.jmii.2022.08.011.